# CEA
## C.E. SACLAY
### DSM

# SERVICE DE PHYSIQUE NUCLÉAIRE

# SHOWER COUNTERS FOR SLAC EXPERIMENTS E142/E143

H. Borel, P. Grenier, J. Lemeur, R. Lombard,
J.C. Lugol, J. Marroncle, J. Morgenstern,
J.P. Mouly, B. Paul, F. Staley, Y. Terrien,
V. Breton, C. Comptour, M. Crouau,
H. Fonvieille, Y. Roblin, G. Savinel,
R.A. Gearhart

# DAPNIA

Le DAPNIA (Département d'Astrophysique, de physique des Particules, de physique Nucléaire et de l'Instrumentation Associée) regroupe les activités du Service d'Astrophysique (SAp), du Département de Physique des Particules Elémentaires (DPhPE) et du Département de Physique Nucléaire (DPhN).

Adresse :        DAPNIA, Bâtiment 141
                    CEA Saclay
                    F - 91191 Gif-sur-Yvette Cedex

Contribution présentée par J. Marroncle pour

les collaborations E142 et E143 aux :

IEEE 1994 Nuclear Science Symposium and Medical

Imaging Conference

Norfolk, Virginia, U.S.A.

du 30 octobre au 05 novembre 1994

# Shower Counters for SLAC Experiments E142/E143

H. Borel, P. Grenier, J. Le Meur, R. Lombard, J.C. Lugol, J. Marroncle,
J. Morgenstern, J.P. Mouly, B. Paul, F. Staley, Y. Terrien
CEA – DAPNIA/SPhN – C.E. de Saclay – F 91191 Gif-sur-Yvette Cedex, France.
V. Breton, C. Comptour, M. Crouau, H. Fonvieille, Y. Roblin, G. Savinel
LPC IN2P3/CNRS, Université Blaise Pascal, F 63170 Aubière Cedex, France.
R. Gearhart: Stanford Linear Accelerator Center, Stanford, CA 94309, USA.

## Abstract

We briefly describe the two electromagnetic calorimeters each made of 200 lead glass blocks used at SLAC to discriminate between electrons and pions and to measure electron energies. Procedures to reconstruct electron showers and to calibrate calorimeters are treated as well as the calorimeter performance.

## I. INTRODUCTION

We are involved in an experimental program of measurements of the spin structure functions $g_1$ and $g_2$ of the nucleon, undertaken at the Stanford Linear Accelerator Center (SLAC). Experiments consist of scattering of longitudinally polarized electrons from polarized targets ($^3$He, $NH_3$ and $ND_3$) in the "Deep Inelastic Scattering" region. The functions $g_1$ and $g_2$ describe the spin structure of the nucleon in terms of its quark and gluon constituents. We evaluate them by measuring the asymmetry in scattering $e^-$ with their spin parallel and anti-parallel to the beam direction. Up to now, we performed two experiments: E142 [1] with electron beam energies of 19 to 25 GeV and E143 [2] at 29 GeV. In the near future, we plan to study $g_1$ and $g_2$ at 50 GeV beam energy (E154 and E155).
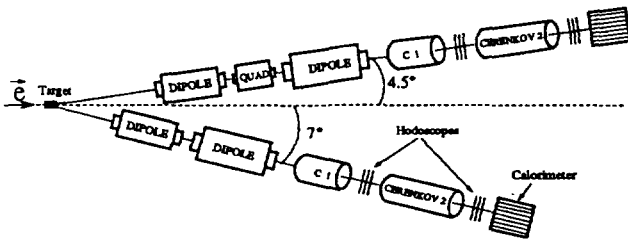


Figure 1. Experimental setup for E142 an E143 experiments.

Electrons are detected independently at two scattering angles in order to increase statistics and enlarge the kinematical domain (see figure 1). In these spectrometers dipole magnets provide dispersion, allowing a momentum determination (P) with a set of six hodoscope planes, particles pass through 2 Cerenkov tanks firing the trigger and allowing us to partially

discriminate $e^-$ from $\pi^-$ especially for P < 9 GeV/c. Particles finish their travel in a lead-glass electromagnetic calorimeter which has a very good rejection power and also a reasonable energy resolution for electrons. This article is devoted to the associated electronics, calibration procedure, energy reconstruction algorithm and performance of these calorimeters.

## II. PRINCIPLE

A high energy electron (E $\gtrsim$ 1 GeV) mainly loses its energy by electromagnetic processes (bremsstrahlung and $e^+$-$e^-$ pair production), developing an electromagnetic shower in heavy materials such as lead glass [3]. In such transparent material with a high refractive index (typically 1.6), the produced $e^+$-$e^-$ pairs emit a large number of Cerenkov $\gamma$ rays, proportional to the number of pairs or, equivalently to the incident particle energy. By collecting these $N_\gamma$ Cerenkov photons with a photomultiplier, we can get a signal which provides us the energy. The width of the signal behaves as $1/\sqrt{N_\gamma}$ or $1/\sqrt{E}$, which means that the energy resolution will be improved for higher energy. On the other hand, a hadron such as a $\pi^-$ leaves only a small part of its energy in such a calorimeter, which allows us to discriminate in most cases $e^-$ from $\pi^-$ just by the amount of energy lost in the lead glass.

Our shower counter is thus used to fullfil two goals:

– $\pi^-/e^-$ rejection: for each particle we compare its energy given by the calorimeter with its momentum (P) reconstructed from hodoscope signals. For an electron the ratio E/P is expected to be close to 1, while for most $\pi^-$ E/P << 1.

– energy measurement: important not only for the rejection but also to have energy information in case where background rates are too high for the hodoscopes to provide a reliable measure of P.

So it appears that a good rejection is synonymous with good energy resolution; pollution due to $\pi^-$ in the electron E/P peak decreases as the width of the peak decreases. As we shall see, the geometrical shape of the shower in the calorimeter can also help us to discriminate $e^-$ from $\pi^-$, this technique being especially useful for events without momentum information.

## III. DESCRIPTION

The calorimeters are made of 200 (20 rows of 10 blocks) lead glass bars. Each bar is of Schott type F2, $6.2 \times 6.2 \times 75$ cm$^3$ size, having a radiation length of 3.17 cm and a refractive index of 1.58 [4]. The blocks are arranged in a fly's eye configuration and stacked upon each other without any gap. They are each read out on one end by a photomultiplier (see figure 2).
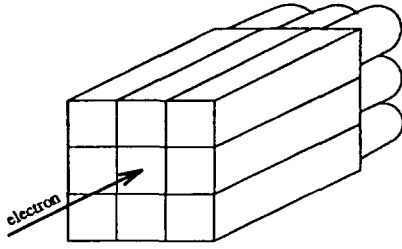


Figure 2. A calorimeter is made of 200 lead glass blocks stacked as illustrated.

The beam was operated at repetition rate of 120 Hz, with a pulse of 1 to 2 $\mu$s length. Data from the CAMAC electronics were written on tape only once a burst. The beam intensity was adjusted to have roughly 2 electrons per burst in the 4.5° spectrometer, and < 0.5 per burst in the 7° spectrometer. Describing trigger distribution by a Poisson law, it appears that we need to register up to 4 triggers per burst to minimize systematic effects on the measured asymmetry.
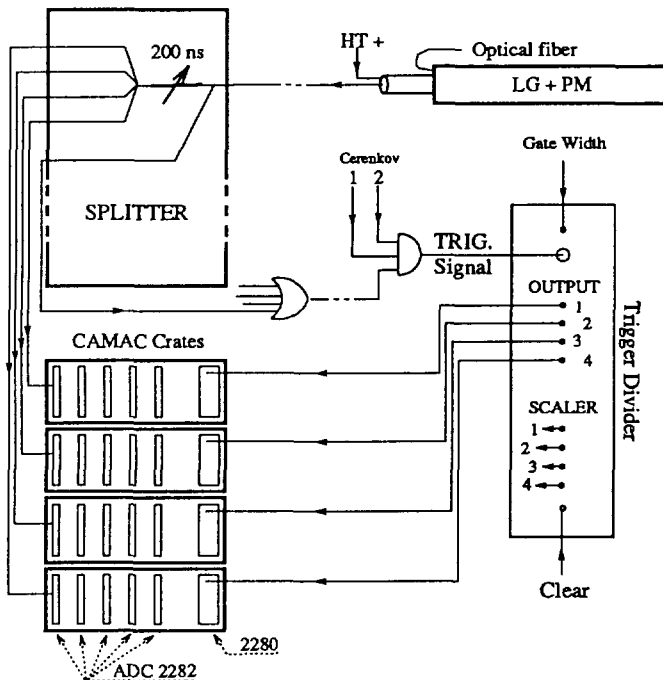


Figure 3. Associated lead glass electronic; splitters; "trigger divider"; ADC; etc ... (see text).

The scheme used to obtain up to 4 triggers per burst is illustrated in figure 3. Each photomultiplier signal is split into five by a simple custom-made splitter circuit. Four of the outputs each representing 18% of the input are delayed by 200 ns, the other one which is 17% is used in the trigger signal and scalers. Information from the photomultipliers is digitalized and coded by Lecroy's 48 channel ADC model 2282 , each driven by one Lecroy 2280 controller which receives the gate signal. In total, we have, per spectrometer, four CAMAC crates with five 2282 ADC modules and one 2280 controller each. An important part of this chain is a custom-made electronic circuit called "trigger divider", which manages the acquisition system. It receives as input the trigger signals of the experiment; for the first one of a given beam spill, it provides a signal gate on its output number 1 to the 2280 of the first CAMAC crate, and only this one. All ADC information from the crate are read out by the data acquisition system and an associated scaler is also incremented. For the second trigger of the same beam spill, if any, only output number 2 is triggered which, causes ADC of the second CAMAC crate to be processed, and so on up to the fourth trigger, if any. One more scaler gives us the number of triggers when more than four occurred in a given spill. Finally a "clear" signal resets the "trigger divider" at the end of the spill. By a level voltage input, the "trigger divider" provides the possibility to work with 2 different lengths of the delivered gate, a short one of 100 ns for physical events and a long one of 500 to 600 ns used by the test system. The dead time of the "trigger divider" is roughly 5 ns, which is lower than dead time due to the electronics of the experimental setup ($\simeq$ 20 ns).

The test system was developed to be able to independently check if each lead glass is working or not. A high intensity Xe flash lamp for each calorimeter (Hamamatsu L2360 ; $\lambda\sim$ 240 – 2000 nm) delivers a luminous signal dispatched to each block through a bundle of plastic optical fibers. A monitoring photomultiplier read out one of the fibers as well as an Am source signal, allowing us to follow fluctuations due to Xe lamp intensity, or gain changes by looking at a possible shifts between the peaks. Such a lamp provides at a rate of 100 Hz a very high luminous signal attenuated by a filter; the width (F.W.H.M.) is roughly 120 ns with a 80 ns rise time. An ADC gate of 250 - 300 ns is enough to integrate the Xe signal but the source signal requires a 500 - 600 ns which is the gate width delivered by the "trigger divider" for "calibration" runs.

## IV. CALIBRATION

The aim of the calibration is to determine for each block and for its 4 associated triggers the correspondence between ADC channel and deposited energy, leading to 200×4 calibration factors per spectrometer. Unfortunately, we could not calibrate each block in a monoenergetic beam, so we used the momentum of electrons measured by the hodoscope system from the experimental data.

Due to the segmentation of the calorimeter, the electromagnetic shower is mostly contained in 9 blocks: the central

block with the higher amount of deposited energy varying between 30 and 90% of the incident energy as shown on figure 4, and the remaining being shared in the 8 surrounding blocks. $E_{central}$ is the energy deposited in the central block. To more accurately find the cluster i.e. lead glass blocks containing significant shower energy, we developed a new clustering method based on "cellular automaton" techniques [5]. Briefly, a cellular automaton is an array of simple individual processing cells, such as ADC signals in our case. To avoid background, such as pedestal fluctuations, we take into account only blocks with energy greater than 50 MeV. This iterative process starts with experimental cell energies as input for the first step, then they evolve according to neighboring cells and some simple rules until final state is reached. This technique has the advantage, compared to the original method which simply used the central blocks and the 8 surrounding ones, to be able to very reliably separate two clusters as long as their central blocks are not adjacent.
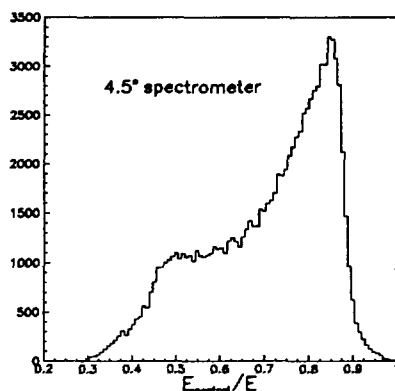


Figure 4. $E_{central}/E$ distribution. The bump at 0.5 is due to the square cross section of lead glass blocks.

To calibrate, we used this cellular automaton and events passing the following criteria:

- the percentage energy deposited in the central block is greater than 65%. This is to be more sensitive to the calibration factor of this block itself and to minimize energy contribution from the surrounding ones.

- cuts in timing and in phase space, which ensure a reliable momentum measurement.

- central block energy must be greater than 5 GeV to reduce as much as possible $\pi^-$ contamination, since $\pi^-$ rates increase rapidly as momentum decreases.

- particle has to be selected as an electron according to the neural network (next paragraph).

This is important in our case, to note that momentum is our only reference for calibration. For each trigger level and each lead glass block, the E/P distribution is examined and we obtain a peak which ideally should be centered at 1 for electrons. Each distribution was fit by a Gaussian function and a new calibration factor was calculated to fulfill this requirement. The procedure was repeated until all E/P distribution converged to 1. To take into account some changes in ADC

gain, magnetic setting, etc ... we need several calibration sets to cover both experiments. Figure 4 shows E/P distributions for a run not used in the calibration procedure; the Gaussian fits for all blocks are centered at 1 and have widths of 5.2% and 5.4% rms for the 4.5° and the 7° spectrometers, respectively.
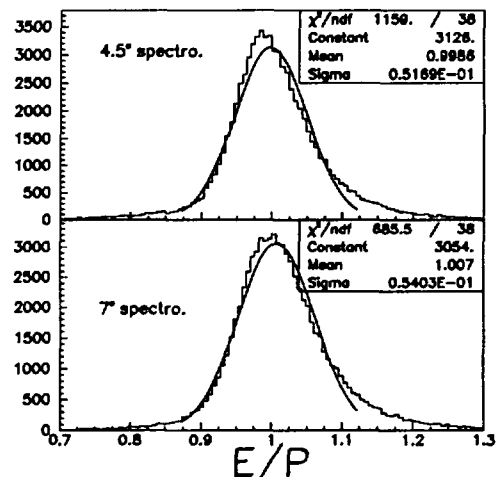


Figure 5. E/P distributions for the 4.5° and 7° spectrometer with their Gaussian fits, for scattered electron energies between 7 and 22 GeV for an E143 run with 29.2 GeV incident energy.

## V. DISCRIMINATION $e^- / \pi^-$

Contamination from $\pi^-$ can be found in the E/P $e^-$ peak since $\pi^-$ interactions in the lead glass can produce $\gamma$, $e^-$ or $e^+$ which then initiate an electromagnetic shower. Such events are not common but one needs to subtract them.

A Neural Network (NN) has been used to discriminate $e^-$ from $\pi^-$ using only the information from the calorimeter. The neural network method is a problem-solving procedure which learns from real or simulated data. Each neuron associates to its input an output calculated by a transfer function which is the same for all neurons. A multilayered feed forward neural network has 1 input layer, 1 output layer and one or several hidden layers of neurons. In this way, output layer neurons are connected to input neurons. In our case, we use 13 neurons on the input layer, each neuron being associated with a variable characterizing a cluster. The total energy is the most important neuron input and the others inputs are: the energy of the central block, the eight energies of the surrounding blocks, the ratio $E_{central}/E$, the deposited energy in the 16 second neighboring blocks and the number of blocks in the cluster. The network output is close to −1 when the cluster was identified as due to a $\pi^-$ and +1 when the network identifies it as coming from an $e^-$ shower. So, training of neural network consists of determining weight values, associated to each link, that best recognize an $e^-$ from a $\pi^-$. We trained the neural network with two samples of GEANT-simulated $e^-$ and $\pi^-$ events and after some iterations, we obtained the weight values. Then, the neural network efficiency is checked on independent samples.
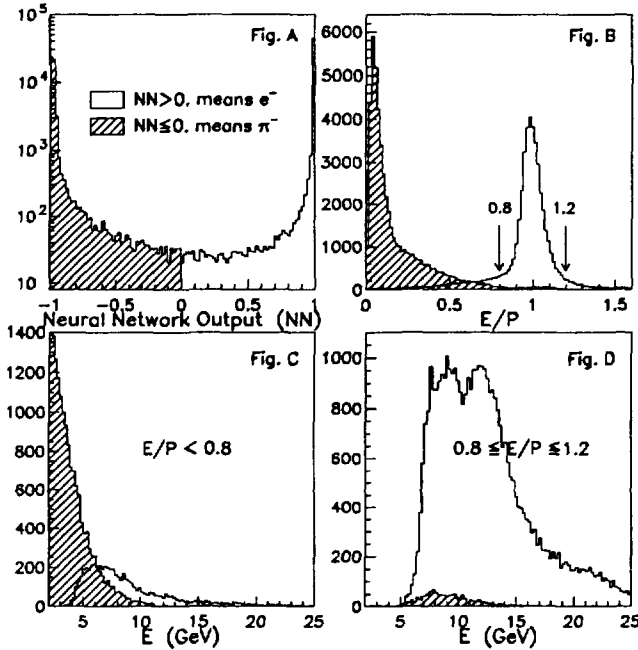
Figure 6. A) neural network output distribution; B) E/P distribution NN>0 and NN<0; C) energy distribution for E/P<0.8; D) energy distribution for $0.8 \leq E/P \leq 1.2$.

Experimental results are shown in figure 6. On 6-A is plotted the distribution of neural network output, showing the $e^-$ for positive NN values (white area) and $\pi^-$ for negative values (hatched area). We can see the efficiency in figure 6-B where the E/P distribution exhibits a clear $e^-$ peak centered at 1; note that $\pi^-$ contamination is very small. When momenta are available, an E/P cut is a nice criterium to discriminate $e^-$ from $\pi^-$, $0.8 \leq E/P \leq 1.2$ for $e^-$ and E/P<0.8 for $\pi^-$. Figures 6-C and 6-D show energy distributions for particles for both previous cuts and give an idea of the contamination distribution and also of the remarkable discrimination power of the neural network. Let us emphasize that this neural network method is able to work efficiently without any knowledge of P. This point is one of the biggest advantages of this method and permits us to recover 6% of the a priori lost events.

# VI. RESULTS

Let us now discuss the results that we have obtained from real data taken at 29 GeV incident energy (E143 experiment).

Some systematic effects have been found with our calorimeters and figure 7 summarizes two of them. The average E/P ($\langle E/P \rangle$) behavior versus $E_{central}/E$ for different energy bins is plotted on this figure. The upper and lower plots are for two lead glass blocks, that view substantially different E ranges. Two features appear clearly. The first is the fact that $\langle E/P \rangle$ increases as $E_{central}/E$ decreases i.e. when the lead glass is hit on its edges. The second is the fact that this effect is bigger for higher energies. Below 10 GeV, the behavior is

roughly flat. An explanation of both effects can be proposed in the following remarks: between lead glass blocks, there are air gaps all the bigger because the blocks have extruded (not polished) surfaces. When an $e^-$ hits lead glass on its edges,
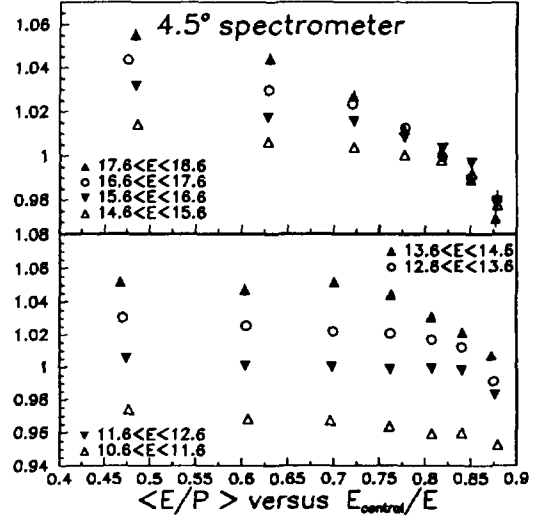


Figure 7. $\langle E/P \rangle$ versus $E_{central}/E$ for different energy bins for two lead glasses (upper and lower figure).

some $e^-$ from shower travel through the air gap before reaching another lead glass block. Thus, these $e^-$ radiate $\gamma$ Cerenkov light closer to the photocathode than they might otherwise, and have therefore more chance to be detected because light attenuation in lead glass is not negligible, and reflections on surfaces are less frequent. So, for a given energy, an electron which hits lead glass close to its edges will be seen as a higher energy $e^-$ than one hitting in the center of the same block.
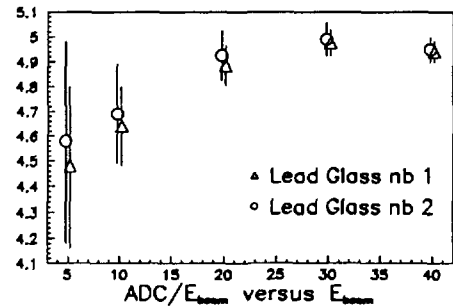


Figure 8. ADC/E versus $E_{beam}$ for two lead glasses. Errors bars are calculated with 2 ADC channel error on each point.

We did an experiment at CERN which was designed to study light attenuation in lead glass. We sent $e^+$ of different energies on the center of two lead glass blocks and, if we plot the ratio of ADC to incident energy versus this energy, we do not observe a horizontal line as expected if attenuation is negligible. These results are plotted on figure 8 and give a clear signature of an attenuation. Thus, two $e^-$ of different energy initiate showers in lead glass deeper for higher energies, increasing in this way the probability to collect $\gamma$ on the

photocathode. This explains why the average $\langle E/P \rangle$ increases with E for the data shown in figure 7 and 9. Simulation with the GEANT code is in progress to reproduce these effects, but results are not yet completely satisfactory.
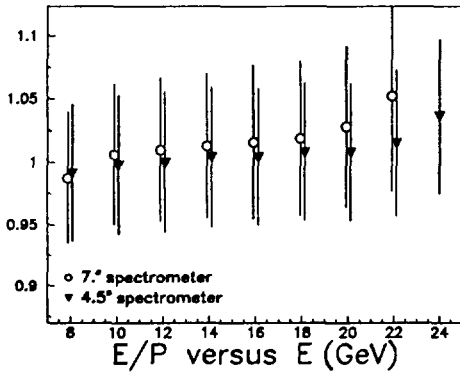


Figure 9. $\langle E/P \rangle$ ratio versus E for both calorimeters. The error bars are the 1-sigma widths from Gaussian fits to the E/P spectra.

The $\langle E/P \rangle$ ratios obtained from the E143 experiment are plotted in figure 9 for both spectrometers; error bars are the 1-sigma widths given by Gaussian fits. We see that the energy calibration is better for the 4.5° calorimeter than for the 7° calorimeter, the 4.5° spectrometer curve being more flat. This is due, in part, to the fact that the correlation between e⁻ momenta and their impact position at the calorimeter is much more important for the 4.5° than the 7° spectrometer (since the former has a focusing quadrupole) which leads to a larger energy range for lead glass blocks belonging to the 7° than those belonging to the 4.5° spectrometer. So when we calibrate
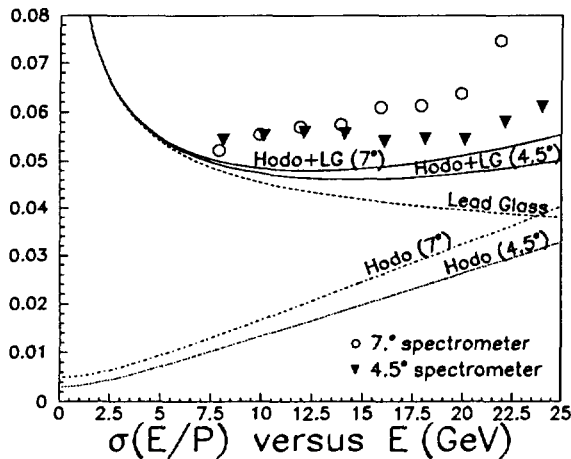


Figure 10. $\sigma(E/P)$ versus E for both calorimeters. Expected contributions from tracking ("hodoscope"), from lead glass and from both combined ("hodo.+LG") are also shown.

a lead glass, $\langle E/P \rangle$ is equal to 1 for the mean value of the energy ($\langle E \rangle$) of this block and differs for other energies by an amount corresponding to the energy range seen by this block.

Thus, $E < \langle E \rangle$ leads to $\langle E/P \rangle < 1$ while $E > \langle E \rangle$ leads to $\langle E/P \rangle > 1$ (see figures 7 and 8). This also explains why $\sigma(E/P)$ for 4.5° must be less than $\sigma(E/P)$ for the 7° spectrometer. Figure 10 shows this, except at low energy where contamination of e⁻ by π⁻ in the 4.5° is significant, introducing some bias in the E/P distributions. Note that the counting rate in the 4.5° is roughly three times that of the 7° calorimeter. Figure 10 also shows the expected tracking contribution to the E/P resolution, indicated by "hodo (4.5°)" or "hodo (7°)", as well as lead glass contribution to this quantity quoted "lead glass" and the quadratic sum of both ("hodo+LG"). The hodoscope contribution is parametrized [6] by $\frac{\Delta P}{P} = \sqrt{0.003^2 + \left(\frac{0.015}{11.5} P\right)^2}$ and by $\frac{\Delta P}{P} = \sqrt{0.005^2 + \left(\frac{0.02}{12.5} P\right)^2}$ for the 4.5° and the 7° spectrometer, respectively, while shower part is given by $\frac{\Delta E}{E} = 0.025 + \frac{0.065}{\sqrt{E}}$. This last contribution was obtained at CERN using e⁺ beams of energy 5 to 50 GeV impinging on a variety of lead glass positions. We see that our experimental results for $\sigma(E/P)$ are about 20% above the "theoretical" parametrization (full curves in figure 10). Studies have shown that most of this discrepancy is due to tracking and/or high background rates. For low luminosity runs, the prediction is in good agreement with the observed E/P peak widths, indicating that the intrinsic tracking and calorimeter resolutions are fairly well understood.

# VII. CONCLUSION

Two calorimeters made of 10×20 lead glass blocks are used at SLAC to discriminate e⁻ and π⁻ by measuring deposited energy. Sophistical tools are developed to calibrate the blocks, to identify energy clusters and to distinguish e⁻ from π⁻. An intrinsic resolution formula is given and despite some systematic effects and high beam intensity, the calorimeters seem to follow the predicted behavior.

We express our gratitude to P.E. Bosted for fruitful discussions.

# VIII. REFERENCES

[1] P.L. Anthony et al., Phys. Rev. Lett. 71, pp. 959, 1993.

[2] K. Abe et al., "Precision Measurement of the Proton Spin Structure Function $g_1^P$", SLAC-PUB-6508, August 1994 T/E, submitted to Phys. Rev. Lett.

[3] R. Wigmans, "Principes et thecnique de calorimétrie", Ecole Joliot-Curie du 26-30 septembre 1988, pp. 163-248, 1988.

[4] G.T. Bartha et al., Nucl. Instrum. Meth. A275, pp. 59-70, 1989.

[5] V. Breton et al., "Application of Neural Networks and Cellular Automata to calorimetric problems", report n° PC-CFRI9405, 1994, submitted to Nucl. Instrum. Meth.

[6] G.G. Petratos, private communication.